Numerical Study of Heat Transfer on Confined Under-Expanded Impinging Jet from Slot into a Plenum

Tinglong Huang, Lianjie Yue, and Xinyu Chang

Abstract The aerodynamic thermal loads on under-expanded jet from bleed slot into a plenum are obtained at different conditions. It grossly differs from the unconfined impinging jet due to the appearance of left-confined wall. The numerical results show that at low slot angle, heat flux along impinging wall peaks twice due to the stagnation of high enthalpy flow and the shock wave/boundary layer interactions, whereas only one peak occurs at higher slot angle due to the former mechanism. When impingement angle is larger than 50°, the highest thermal loads change a little. As the impingement height increases, the overall aerodynamic thermal loads decrease at the same freestream conditions. Generally, it is the confined wall that makes the flow behind the plate shock supersonic, which allows the SWBLIs to occur.

1 Introduction

The internal flow path features some complex flow phenomena. Different types of irreversible processes are involved, such as shocks and shock-induced boundary layer separations [1]. As one of the most powerful methods to suppress boundary layer separations, the bleed systems were introduced into scramjet design. However, the bleed slots would suffer from aerothermal load at hypersonic conditions although the bleed can even reduce vortex-induced highly localized thermal loads by eliminating the boundary layer separation [2]. Yue et al. [3] found, besides the maximum thermal load at the stagnation point of the bleed corner, a localized high heat flux occurred within the slot passage, attributed to a boundary layer separation triggered by the bleed barrier shock. But aerodynamic thermal load on solid surfaces, caused by under-expanded jet from bleed slot impinging into a plenum, is still unclear. Under-expanded impingement jet can induce high heat

T. Huang · L. Yue (✉) · X. Chang
Institute of Mechanics, Chinese Academy of Sciences, Beijing, China
e-mail: yuelj@imech.ac.cn

A. Sasoh et al. (eds.), *31st International Symposium on Shock Waves 2*,
https://doi.org/10.1007/978-3-319-91017-8_147

transfer rate on the impinged surface, which would be severe in fully confined hypersonic bleed slot systems.

Under-expanded supersonic impinging jet has attracted many investigators' attention due to high heat transfer rates in the impingement zone. The mean flow visualization and properties, including pressure distributions and heat transfer rates, and the instantaneous flow field of axisymmetric or two-dimensional impingement jet have been studied extensively [4–7]. It was revealed that the jet impingement essentially depends on the following parameters, the ratio of total pressure and ambient pressure *Pt/Pa*, the jet-to-plate distance *h/d*, and impingement angle θ. Donaldson and Snedeker [4] noted that the impinging flow field can be generally divided into three regions, including the primary jet flow region upstream the strong interaction effects of impingement, the impingement region, and the wall jet region. The impingement region sometimes appears a stagnation bubble [8, 9]. For highly under-expanded impinging jet, a Mach disk occurs and interacts with jet shock. For oblique jet impingement, Yusuke et al. [10] classified the flow pattern into three types by the observation of shock wave configurations and the pressure maps, which can be estimated based on θ and *h/d*, and the shock cell length of corresponding free jet. Song et al. [11] observed that the low recovery factor region moves downstream and the cooling/heating effect declines overall as θ decreases.

Although in-depth understanding has been achieved regarding the impingement jet flow, aforementioned works mainly focus on the unconfined jet impingement. In the bleed system, the impingement jet flow characteristics would be much different due to the geometric confinement. It is necessary to investigate the flow patterns and the associated aerodynamic thermal loads for the fully confined under-expanded supersonic impinging jet.

2 Numerical Method and Computational Details

2.1 Numerical Methods

The steady-state Reynolds-averaged Navier-Stokes equations are solved for two-dimensional turbulence flow by using commercial code CFD++. The turbulence model of k-ω SST is employed to enclose the governing equations. Our previous studies have verified that the adopted numerical algorithm is very credible and can efficiently resolve high Mach number flows and aerodynamic heating, including type IV shock interference and shock wave/boundary layer interactions [3, 12, 13].

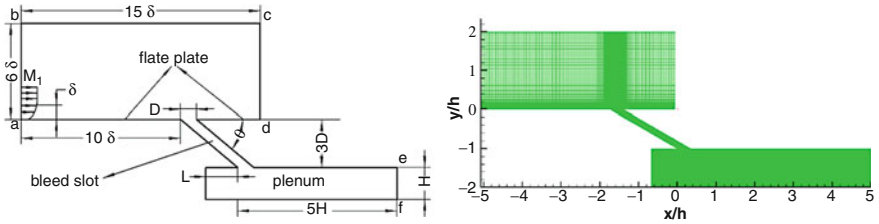

Fig. 1 Computational domain, grid mesh distribution

2.2 Computational Details

Figure 1 shows the solution domain used in our two-dimensional simulations. It includes three regions, a region above the plate, a bleed slot, and a plenum. The conjunction of two walls is simply a sharp corner. At the inflow boundary a-b, a freestream high enthalpy airflow with $T_t = 1824.5$ K, $Ma_1 = 4$, $p_1 = 22{,}755$ Pa, and $Re = 1.071 \times 106\ \mathrm{m}^{-1}$ is imposed, which approximately corresponds to the flow conditions in the internal contraction section of hypersonic inlets operating at flight Mach number of 6 and altitude of 26 km [3]. Bleed systems are usually installed around this section [2, 14, 15]. The inflow boundary a-b has a turbulent boundary layer with stream-wise velocity profile described by the Van Direst profile with one-seventh power law, where the boundary layer thickness δ is 2.5 mm. At the outflow boundary c–d, all flow parameters are extrapolated from interior region. At the plenum outflow boundary e–f, a back pressure boundary which allows reversed flow is applied. At all solid surfaces, no-slip isothermal temperature conditions are imposed, where $T_w = 300$ K.

Quadrilateral structured cells are used in the simulation as shown in Fig. 1. The first mesh size normal to the wall is 1 μm, corresponding to $y + < 1$ on the solid surface. The grid number in turbulent boundary layer is greater than 50 so as to resolve the temperature gradient well. The total number of mesh grids is about 0.18–0.25 million.

3 Numerical Results and Discussion

The flow patterns and aerodynamic thermal loads on the wall are discussed in the present section. Slot angle is changed from 30° to 90°. Detailed flow patterns and aerodynamic thermal loads within the bleed slot region were studied by Yue et al. [3]. Present works will pay more attention to the plenum region. In the following discussions, the local heat flux rates are nondimensionalized with respect to freestream conditions:

$$St = \frac{q_w}{\rho_1 U_1 C_p (T_t - T_w)} \tag{1}$$

where q_w, ρ_1, U_1, C_p, T_t, and T_w denoted the local heat flux on the solid surface, freestream density, freestream velocity, local specific heat, total temperature, and wall temperature, respectively.

3.1 Effects of Slot Angle on Aerodynamic Thermal Loads

Figure 2 shows the Mach contour in the plenum region with different slot angles where $h/d = 3$ and the back pressure on the exit of plenum doesn't exert influence on the upstream flow. Figure 3 shows the schematic picture of flow structures in the plenum region. At $\theta = 30$–$40°$, on the left of plenum are two large recirculation regions R1 and R2 with opposite rotation direction. On the middle, a shock (plate shock wave) over the impinged wall occurs. The plate shock induces the recirculation region SB1. An incident shock wave occurs in the core flow region and intersects with plate shock. The transmitted incident shock interacts with boundary layer on the impinged wall and induces a separation bubble SB. Between the separation bubble SB and SB1 is an aerodynamic throat. For $\theta > 40°$, the separation bubble SB disappears. At $\theta = 90°$, the left two recirculation regions combine and lead to secondary impingement to the left-confined wall.

The corresponding Stanton number distributions along the impinged surface at $\theta = 30°$ are shown in Fig. 3. There are two peaks of heat flux on the impinged wall. The left heat peak is relatively small and is considered to be generated by the stagnation of the supersonic flow. The right heat peak locates at the reattachment point of separation bubble induced by incident shock and is the highest heat flux

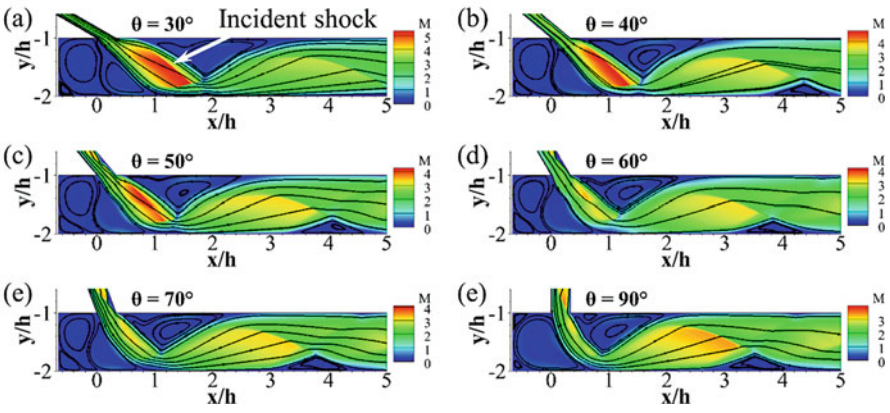

Fig. 2 Mach contour map on the plenum at various slot angles

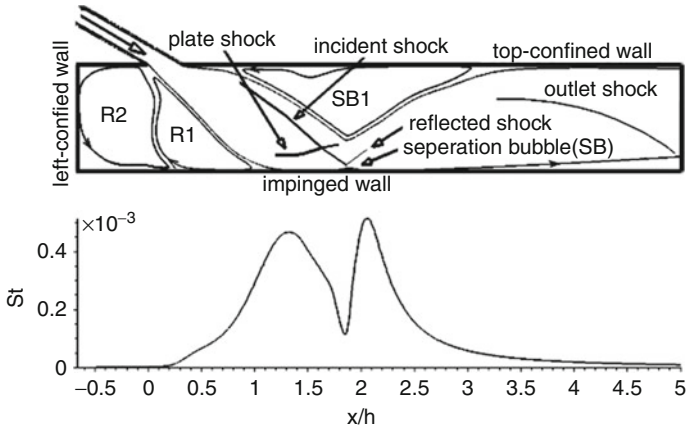

Fig. 3 Schematic of flow structures, St distributions on the impinged wall at $\theta = 30°$

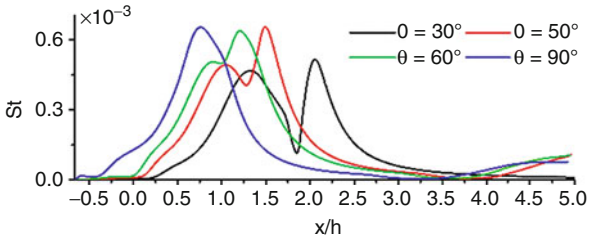

Fig. 4 Stanton number distributions on the impinging wall at various slot angles

peak due to the SWBLIs. Near the recirculation region R2, the heat flux is low which indicates the difficulty of the high enthalpy flow to reach this region.

The St number distributions along the impinged wall are presented in Fig. 4. For $\theta = 30$–$60°$, the oblique impinging jet generates two peaks. And the first peak is 0.00047, 0.00051, 0.00049, and 0.00051, respectively. It changes a little as the slot angle increases as indicated. The second peak due to SWBLIs is 0.00052, 0.00073, 0.00066, and 0.00064, respectively. For $\theta = 70°$ and $90°$, only one peak appears on the impinged wall. Their maximum values of St number are 0.00061 and 0.00065, respectively. Comparing all the highest peaks at various slot angles, the highest heat flux peak changes a little when $\theta > 50°$.

The St number distributions along the top-confined wall and left-confined wall are shown in Fig. 5. The local maximum heat flux appears on the reattachment position of the recirculation region SB1. These peaks are 0.000227, 0.000252, 0.000263, 0.000224, 0.000249, and 0.000223, for $\theta = 30$–$90°$, respectively. The highest of these peaks is about 44% of the corresponding highest St on impinged wall. At the corner of the slot exit, it is always a high thermal load area due to the high transport speed of jet flow and small blunted radius. For the left-confined wall, the maximum heat flux rate is no more than 3% of heat peak on impinged wall for $\theta < 90°$ due to the low-speed separated flow in this region. At $\theta = 90°$, the thermal

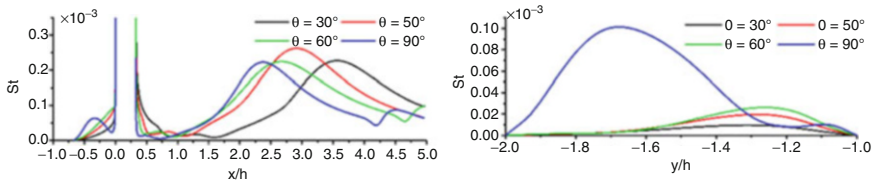

Fig. 5 St number distributions at various θ on top-confined wall, left-confined wall

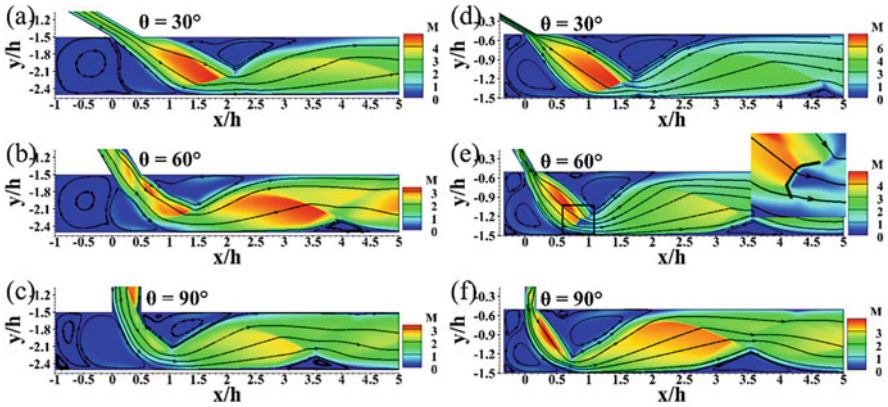

Fig. 6 Mach number contour map at various θ and at $h/d = 2$ (a, b, c), 6 (d, e, f)

loads increase dramatically due to the subsonic jet impingement. But the peak heat flux is still no more than 16% of the one on impinged wall.

3.2 *Effects of Plenum Height*

To investigate the effects of plenum height on aerodynamic thermal loads, three typical slot angles, $\theta = 30°$, 60°, and 90°, and ratio of $h/d = 2$, 3, 6 are selected to extensively discuss. Figure 6 shows that the flow patterns change a little as h/d increases. When the plenum height increases, the remarkable change is the appearance of Mach stem structure at $h/d = 6$ and $\theta = 60°$.

Figure 7 shows that for a same θ, almost all distributions maintain the same profile for different h/d, but the maximum St number decreases as h/d increases due to the drop of the capacity for energy transport.

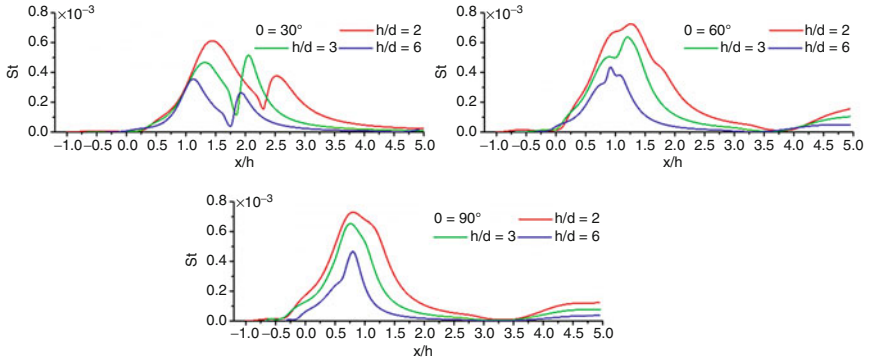

Fig. 7 Stanton number distributions on the impinging wall at various θ and h/d

4 Conclusions

A two-dimensional numerical investigation is conducted to study the aerodynamic thermal loads on the surfaces of plenum of bleed systems in high enthalpy flows. Bleed slot angle and plenum height are chosen to examine the influences of the appearance of confined wall. Numerical results show that due to the confinement of confined wall, several recirculation regions occur. In addition, the shock wave boundary layer interactions (SWBLIs) play an important role on heating the plenum and bleed slot surfaces. In this fully confined supersonic impinging jet flow, the mechanism of aerodynamic heating is mainly the same as the reattachment position of separation bubble induced by SWBLI effects.

At fixed freestream conditions, for lower bleed slot angle, a key separation bubble is induced by SWBLIs over the impinging wall, resulting in a maximum heat flux at the reattachment position. As the slot angle increases, the maximum and averaged heat flux increases.

When the plenum height increases, the flow patterns change a little except the case with $\theta = 60°$ and $h/d = 6$. In this special case, Mach stem occurs due to the overlarge deflection angle. However, the overall thermal loads reduce as h/d increases due to the decrease of mass flow.

References

1. J. Häberle, A. Gülhan, Experimental investigation of a two-dimensional and a three-dimensional scramjet inlet at Mach 7. J. Propuls. Power **24**(2008–09), 1023–1034 (2008)
2. T. Kouchi, T. Mitani, G. Masuya, Numerical simulations in scramjet combustion with boundary-layer bleeding. J. Propuls. Power **21**(4), 642–649 (2012)
3. L. Yue et al., Aerothermal characteristics of bleed slot in hypersonic flows. Sci. China Phys. Mech. Astron. **58**(10), 1–14 (2015)

4. C.D. Donaldson, R.S. Snedeker, A study of free jet impingement. Part 1. Mean properties of free and impinging jets. J. Fluid Mech **45**(2), 281–319 (1971)
5. D. Schulte, A. Henckels, U. Wepler, Reduction of shock induced boundary layer separation in hypersonic inlets using bleed. Aerosp. Sci. Technol. **2**(4), 231–239 (1998)
6. B. Henderson, J. Bridges, M. Wernet, An experimental study of the oscillatory flow structure of tone-producing supersonic impinging jets. J. Fluid Mech. **542**, 115–137 (2005)
7. F. Alvi, J. Ladd, W. Bower, Experimental and computational investigation of supersonic impinging jets. AIAA J. **40**(4), 599–609 (2002)
8. F. Alvi, K. Iyer, Mean and unsteady flowfield properties of supersonic impinging jets with lift plates. AIAA paper **1829**, 1999 (1999)
9. G. Kalghatgi, B. Hunt, Occurrence of stagnation bubbles in supersonic jet impingement flows. Aeronaut. Q. **27**, 169–185 (1976)
10. Y. Nakai, N. Fujimatsu, K. Fujii, Experimental study of underexpanded supersonic jet impingement on an inclined flat plate. AIAA J. **44**(11), 2691–2699 (2006)
11. J. Song et al., Thermal characteristics of inclined plate impinged by underexpanded sonic jet. Int. J. Heat Mass Transf. **62**, 223–229 (2013)
12. H. Lu, L. Yue, X. Chang, Flow characteristics of hypersonic inlets with different cowl-lip blunting methods. Sci. China Phys. Mech. Astron. **57**(4), 741–752 (2014)
13. H. Lu et al., Interaction of isentropic compression waves with a bow shock. AIAA J. **51**(10), 2474–2484 (2013)
14. J. Häberle, A. Gülhan, Internal flowfield investigation of a hypersonic inlet at Mach 6 with bleed. J. Propuls. Power **23**(2007–10), 1007–1017 (2007)
15. T. Mitani et al., Boundary-layer control in Mach 4 and Mach 6 scramjet engines. J. Propuls. Power **21**(4), 636–641 (2005)